SPECT Liver Imaging Using an Iterative Attenuation Correction Algorithm and an External Flood Source

J.A. Malko, R.L. Van Heertum, G.T. Gullberg, and W.P. Kowalsky

Department of Radiology, Emory University School of Medicine, Atlanta, Georgia; St. Vincent's Hospital and Medical Center, New York City, and Department of Radiology, University of Utah, Salt Lake City, Utah

The results obtained from the inclusion of a new intrinsic attenuation correction algorithm into a protocol for SPECT liver imaging are presented in this study. A total of six patients were evaluated with this protocol. The new algorithm uses a transmission tomographic acquisition that is obtained before a standard emission tomograph, and requires the use of an external flood source. The transmission tomograph results in an attenuation image, or map, of the patient. The attenuation map then serves as input into the final intrinsic correction algorithm, that also uses data from a standard emission acquisition. The results of the six patients studied show that the algorithm can correct for attenuation effects without degrading image quality. In all the cases studied, the attenuation corrected images made the cases easier to interpret than did the images obtained without attenuation correction.

J Nucl Med 27:701–705, 1986

An important goal of single photon emission computed tomography (SPECT) is to obtain reconstructed image pixels whose counts are directly proportional to the radionuclide concentration. The single most important effect complicating this goal is the attenuation of photons by surrounding body tissue. While in computed tomography (CT) the reconstructed image results directly from this tissue attenuation, in SPECT the reconstructed image is a reflection of the radionuclide distribution, distorted somewhat by tissue attenuation of the emitted photons. In clinical practice, qualitative SPECT images can be reconstructed and be of some use without attenuation correction. This is primarily because the injected radionuclide compound is usually specifically designed for preferential uptake by the organs of interest relative to the surrounding background. The resulting images, although attenuated, still present well-defined external organ boundaries with respect to background. In SPECT imaging of the liver, for example, the attenuation effects still result in a well-defined liver boundary, but with progressively fewer counts toward the interior of the organ. The resulting image, which for a normal liver presents a "hot rim effect" can, however, cause significant difficulty in discerning central lesions.

In recent years, attenuation correction methods of varying accuracy and sophistication have been developed. The simplest methods apply correction factors to the tomographic data either before the image reconstruction algorithm (preprocessing) (*1–3*), or after image reconstruction (postprocessing) (*4,5*). The preprocessing methods are only accurate when the radionuclide is uniformly distributed throughout a uniform attenuator (*3*). The most exact methods are those that incorporate the attenuation effects directly into the reconstruction algorithm (*6*). These so-called "intrinsic" methods, when combined with a attenuation map of the object being imaged, lead to theoretically exact solutions. In a number of previous publications dealing with comparative studies of various attenuation correction algorithms (*6–8*) we have shown how intrinsic methods lead to improved quantitation when applied to experimental data acquired using a liver phantom. In the following study, we discuss the results obtained from the incorporation of a new intrinsic attenuation correction algorithm (*6*) into a clinical protocol for SPECT liver imaging.

Received June 24, 1985; revision accepted Dec. 31, 1985.

For reprints contact: J. A. Malko, Dept. of Radiology, Emory University Hospital, 1364 Clifton Rd., N.E., Atlanta, GA 30322.

MATERIALS AND METHODS

Algorithm

The new iterative correction algorithm employed here uses the maximum likelihood technique (*9*) to iteratively converge to the optimum solution of the attenuation problem modeled by an attenuated projector-backprojector. Briefly, the SPECT projection and backprojection equations are written explicitly to include the exponential attenuation factors. These equations are then solvable for the initial unattenuated radionuclide distribution if the complete attenuation distribution for the object is known. This attenuation distribution is calculated from a separate transmission tomographic study of the object, obtained through the use of an external flood source. The transmission study is acquired before the SPECT study and before the radionuclide is injected into the patient.

Protocol

A total of six male patients ranging in age from 45 to 78 yr were studied at one of our institutions. Informed consent was obtained from all patients. The data were acquired using a commercial SPECT tomographic system (GE 400A/T) which was modified to permit the attachment of a refillable planar flood source (Fig. 1). This attachment kept the flood parallel to the camera face as the camera and flood were rotated about the patient during the transmission tomographic acquisition. The refillable flood contained a solution of 20 mCi (740 MBq) of sodium technetium-99m (^{99m}Tc) pertechnetate in water. With the patient in a supine position between the camera and flood, a 180°, 64 view, 20 sec/view transmission tomographic acquisition was obtained. The flood was then removed. From this point, the protocol followed the standard protocol for a SPECT liver scan. The patient was injected with 5 mCi (185 MBq) of [^{99m}Tc]sulfur colloid, and 10 min postinjection a 360°, 128 view, 10 sec/view SPECT acquisition was obtained. Both the transmission and SPECT acquisitions were acquired using a 20% energy window. The patient was cautioned to remain as still as possible throughout the transmission and emission acquisitions and the intervening time between the two studies. Approximately 8 hr after the transmission study, the flood was returned to its position opposite the camera face, and a 2-min planar image of the flood was obtained. The purpose of this last acquisition was to obtain a measure of flood source strength. The 8-hr delay was necessary to keep the initial high count rate of the flood from saturating the camera. All of the data were uniformity corrected using a 30 million count flood matrix.

Data Processing

The data were acquired into a commercially available camera-computer system, (GE STAR) and subsequently transferred to an off-line computer (Data General MV8000) for processing. All of the data were decay-corrected for the ^{99m}Tc half-life. For the transmission acquisition, the counts in the projection bins were first redefined as the log of the ratio of the flood source strength divided by the original bin counts.

The flood source strength was obtained from the uniformity and decay corrected 8-hr, delayed image of the transmission flood, and was defined as the average pixel value in the useful field-of-view. The redefined projections were then processed through a standard maximum likelihood algorithm (*9*) to yield attenuation transmission tomographic images. The attenuation images and the raw SPECT data were both used as input into the iterative attenuation correction algorithm, and resulted in attenuation corrected emission images. Finally, for comparison, the SPECT data were processed through a standard nonattenuation corrected ramp-filtered backprojection algorithm, yielding uncorrected emission images. For each patient, three sets of transaxial tomographic images were thus obtained: (a) transmission attenuation images, (b) attenuation corrected emission images, and (c) unattenuation corrected emission images. For display purposes, all the images were

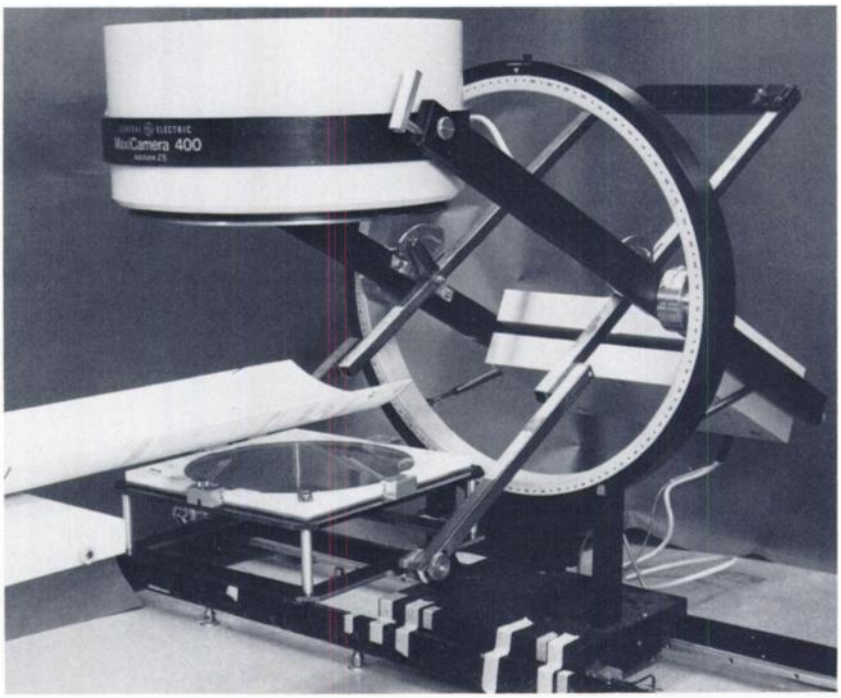

FIGURE 1
Tomographic equipment with external flood attachment used to obtain transmission tomographic data

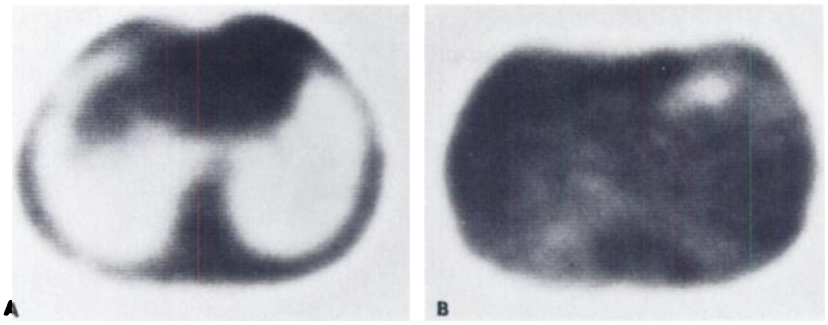

FIGURE 2
Two reconstructed transmission transaxial slices (A, B) from study of Patient 1. Lighter regions correspond to less dense regions

smoothed with a three-dimensional spatial filter equivalent to a 1-2-1 smooth in each dimension.

RESULTS

Two representative transmission transaxial slices for Patient 1 are shown in Fig. 2. These are density images in which the lighter regions correspond to less dense tissue. Slice A passes through the superior portion of the liver; lung, heart, and spine are clearly differentiated. Slice B, which is ~4.5 cm inferior to Slice A, shows an approximately uniform density distribution except for a low-density region that is probably due to gas in the stomach. These density images, without filtering, were used as input into the iterative attenuation algorithm.

Figure 3 shows a selected slice from the iterative attenuation corrected SPECT algorithm for each of the six patients. For comparison, the corresponding unattenuation corrected image for each case is also shown.

Patient 1 was a 78-yr-old man with documented advanced gastric cancer. The study revealed hepatosplenomegaly with multiple photon deficient defects representing metastatic disease in both the right and left lobes of the liver. The uncorrected image tended to exaggerate the extent of disease in the left lobe and central portion of the liver.

Patient 2 was a 45-yr-old man with a long history of heavy alcohol abuse, and resultant alcoholic liver disease. The images revealed a shrunken right lobe, a hypertrophied left lobe, along with a very inhomogenous and diminished radionuclide uptake throughout the liver. In addition, there was augmented uptake in an enlarged spleen. These findings were consistent with the final clinical diagnosis of decompensated cirrhosis with portal hypertension, and were better appreciated on the attenuation corrected images.

Patient 3 was a 73-yr-old male currently admitted with a pure red blood cell aplasia associated with chronic lymphatic leukemia. The patient had a prior negative liver/spleen scan in 1980. The present study demonstrated a low lying liver which was moderately enlarged and had an overall inhomogenous distribution. This inhomogeneity was again more clearly appreciated on the attenuation corrected images.

FIGURE 3
Reconstructed emission transaxial slices for six patients. For each patient image on right (B) is obtained from iterative attenuation corrected algorithm, while image on left (A) is same slice reconstructed using unattenuation corrected algorithm

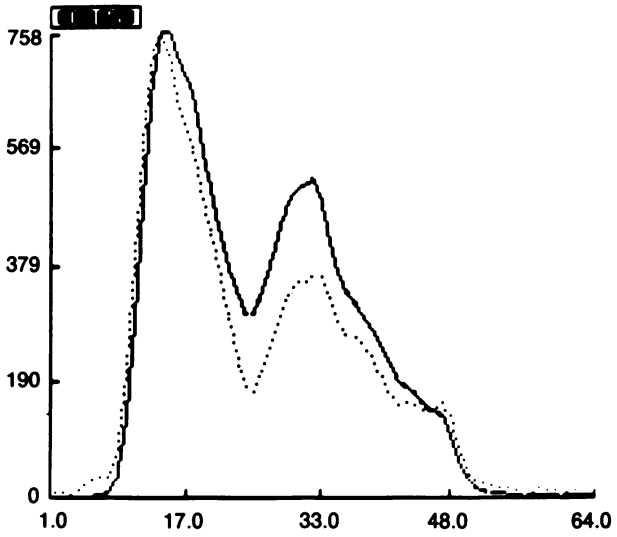

FIGURE 4
Representative horizontal count profile through slice for Patient 6, obtained at same level, for attenuation corrected image (solid curve) and uncorrected image (dotted curve). Profiles have been normalized to same maximum value

The spleen was also moderately enlarged, with augmented radiopharmaceutical uptake.

Patient 4 was a 52-yr-old man with a small-cell carcinoma of the right lung and a long history of heavy alcohol abuse. The images showed an enlarged porta-hepatis which was much more clearly seen on the corrected image.

Patient 5 was a 72-yr-old male with a long history of alcohol abuse and past history of cirrhosis. The patient was recently found to have a tumor of the right kidney. The images showed a homogenous distribution in the liver with an enlarged left lobe and prominent porta-hepatis which was more clearly defined on the attenuation corrected image. The spleen was enlarged and had augmented uptake. Both CT and ultrasound confirmed the negative scan.

Patient 6 was a 67-yr-old male with a long history of alcohol abuse, hepatitis, and i.v. drug abuse. The patient had elevated liver function tests and a 40 lb weight loss. The images showed a normal sized liver and spleen with an enlarged porta hepatis.

DISCUSSION

The results from the six patients studied indicate that the employed iterative attenuation correction algorithm can correct clinically relevant data for the effects of attenuation without degrading image quality. Even in the case of a severely diseased liver (Fig. 3, Patient 1) the algorithm resulted in good image quality with well-defined lesion boundaries and no loss of resolution. As would be anticipated, the elimination of the effects of attenuation led to better identification and delineation of internal structures. In all cases studied, the porta hepatis was more clearly seen in the attenuation corrected images. In general, the iterative attenuation correction made all the cases easier to interpret.

In addition to improved visual interpretation, there is an important added benefit to be gained from this correction algorithm. Although less exact attenuation correction algorithms can also lead to qualitatively useful images, the correction used here should theoretically be quantitatively exact (*6*), and therefore, the resulting image pixel count values are the natural starting point for any further quantitative analysis of the data. The estimation of functioning hepatic volumes is an obvious example of a measurement that would benefit from this approach. A number of different volume algorithms employ a threshold technique in the volume estimation (*10–12*). In a threshold technique, the count level of each image pixel is used to decide if the pixel is to be included in the calculated volume; any correction to the pixel count level can thus effect this calculated volume. Figure 4 shows two horizontal count profiles through the slice for Patient 6, obtained at the same level, for the attenuation corrected slice (solid curve) and the uncorrected slice (dotted curve). A comparison of these two profiles, that have been normalized to the same maximum value, shows quantitatively the difference in pixel count values. A threshold defined as 50% of the maximum pixel in the profile selects 21% of the pixels in the attenuation corrected profile but only 16% in the uncorrected profile, and in addition selects a different shape for each profile. Differences such as these, when applied to the total slice, can lead to differences in calculated slice volumes.

The major drawback of the present protocol is the extra imaging time needed for the transmission study. A collimated flood source is presently under development; its use should allow us to increase the activity in the flood without increasing the dose to the patient, since a large portion of the patient dose from an uncollimated source comes from undetected scattered radiation. The increased activity will allow shorter scan times for the same statistical accuracy. Calculations and measurements we have made show that the present dose to the patient from the transmission acquisition is negligible in comparison to the dose received from the injected radionuclide. We feel that the qualitative and quantitative advantages resulting from the attenuation corrected images will, depending on the case, outweigh the added time and effort needed.

REFERENCES

1. Budinger TF, Gullberg GT: Transverse section reconstruction of gamma-ray emitting radionuclides in patients. In *Reconstruction Tomography Radiology and Nuclear Medicine*, Ter-Pogossian MM, Phelps ME, Brownell GL, et al., eds. Baltimore, University Park Press, 1977, pp 315–342
2. Kay DB, Keyes JW, Jr: First order correction for absorption and resolution compensation in radio-

nuclide Fourier tomography. *J Nucl Med* 16:540–541, 1975
3. Budinger TF, Gullberg GT, Huesman RH: Emission computed tomography. In *Image Reconstruction from Projections: Implementation and Applications*, Herman GT, ed. New York, Springer-Verlag, 1979, pp 147–246
4. Kuhl DE, Edwards RQ, Ricci AR, et al: Quantitative section scanning using orthogonal tangent correction. *J Nucl Med* 14:196–200, 1973
5. Chang LT: A method for attenuation correction in radionuclide computed tomography. *IEEE Trans Nucl Sci* NS-25:638–643, 1978
6. Gullberg GT, Huesman RH, Malko JA, et al: An attenuated projector-backprojector for iterative SPECT reconstruction. *Phys Med Biol* 30:799–815, 1985
7. Gullberg GT, Malko JA, Eisner RL, et al: Application of attenuation correction to clinical data. *J Nucl Med* 23:P84, 1982 (abstr)
8. Gullberg GT, Malko JA, Eisner RL, et al: Application of attenuation correction to clinical data. *General Electric Publication No. 5408*
9. Lange K, Carson R: EM reconstruction algorithms for emission and transmission tomography. *J Comput Assist Tomogr* 8:306–316, 1984
10. Tauxe WN, Soussaline F, Todd-Pokropek A, et al: Determination of organ volume by single-photon emission tomography. *J Nucl Med* 23:984–987, 1982
11. Malko JA, Eisner RL, Engdahl JC, et al: A threshold method of volume determination from tomographic reconstructions. *J Nucl Med* 24:P19, 1983 (abstr)
12. Kawamura J, Itoh H, Yoshida O, et al: In vivo estimation of renal volume using a rotating gamma camera for ^{99m}Tc-dimercaptosuccinic acid renal imaging. *Eur J Nucl Med* 9:168–172, 1984